Electronic Supplementary Material (ESI) for ChemComm.

Isolated Ni atoms catalyst supported on $Ti_3C_2T_x$ with asymmetrical C-Ni-N structure for hydrogen evolution reaction

Haosen Yang,[a] Pengfei Wu,[a] Jiajing Pei,[b] Bo Peng*[c] and Qingqing Liu*[d]

[a] *School of Chemistry, Key laboratory of Bio-lnspired Smart Interfacial Science and Technology, Beijing Advanced Innovation Center for Biomedical Engineering, Beihang Universitv, Beijing, 100191, China.*
[b] *Institute of High Energy Physics, Chinese Academy of Sciences, Beijing 100049, China.*
[c] *Guangxi Key Laboratory of Polysaccharide Materials and Modification, Laboratory of Chemical and Biological Transforming Process of Guangxi Higher Education Institutes, School of Chemistry and Chemical Engineering, Guangxi Minzu University, Nanning 530008, China.*
[d] *School of Physics, Beihang University, Beijing, 100191 China*

Chemicals.

The Ti_3AlC_2 (99%, 400 mesh) and LiF (99%) were purchased from Xiyan Xincailiao Technology Co., Ltd, China. Concentrated hydrochloric acid (HCl, 12M) was obtained from Beijing Chemical Reagents. The chlorides, including $NiCl_2 \cdot 6H_2O$, were purchased from Alfa Aesar. The melamine was purchased from Alfa Aesar. Nafion D-521 dispersion (5% w/w in water and 1-propanol) were obtained from Alfa Aesar. The deionized water used in this experiment with a resistivity of 18.2 MΩ cm^{-1} All the chemicals were analytical grade and used without further purification.

Synthesis.

Preparation of single/few-layer $Ti_3C_2T_x$ nanosheets.

The modified minimally intensive layer delamination (MILD) was used to synthesize $Ti_3C_2T_x$ nanosheets with abundant Ti vacancies.

Firstly, 2 g lithium fluoride (LiF) was slowly added to 40 mL concentrated hydrochloric acid (HCl, 10 M) and stirred slowly in ice water bath, so that LiF was completely dissolved in concentrated hydrochloric acid to form a uniformly dispersed etching solution. The etching solution is kept in an ice water bath, 1 g Ti_3AlC_2 is slowly added to the above etching solution, and then the water bath is heated to 40°C, and etched continuously for 25 hours at 35°C. After etching, the obtained multi-layer $Ti_3C_2T_x$ is washed with hydrochloric acid and deionized water to remove excess LiF and other impurities, and the precipitate can be obtained by washing until the pH is about 6.

Then multi-layer $Ti_3C_2T_x$ was added to a certain amount of deionized water for ultrasonic exfoliation, which was treated in argon atmosphere and ultrasonic in ice water bath for 1 hour. The suspension obtained by ultrasound was centrifuged at 3500 rpm for 1 hour. After centrifugation, the dark green supernatant was collected and labeled as single/few-layer $Ti_3C_2T_x$ nanosheets. The supernatant is frozen and stored. In order to get the powder sample, the frozen sample can be freeze-dried in a freeze-dryer for about 48 hours, solid $Ti_3C_2T_x$.

Preparation of Ni SA@N-$Ti_3C_2T_x$ and Ni SA@$Ti_3C_2T_x$.

50 mg $Ti_3C_2T_x$ was placed in 15 mL deionized water, followed by ultrasonic for 30 min and magnetic stirring for 20 min. Then 5 mg $NiCl_2 \cdot 6H_2O$ and 100 mg melamine was added , and stirred for 1 hour. Then, ultrasound was performed in an ice bath for 30 minutes. The samples were freeze-dried for 48 hours to obtain powder samples. The samples were placed in a tubular furnace for annealing at 750°C for 2 hours in Ar

atmosphere. The obtained samples were washed three times with water and ethanol, respectively. Dry overnight at room temperature in vacuum. The obtained sample was labeled Ni SA@N-$Ti_3C_2T_x$. The same prepared procedure of Ni SA@N-$Ti_3C_2T_x$ was conducted for the synthesis of Ni SA@$Ti_3C_2T_x$ without the addition of melamine.

Characterization.

The morphology and size of the catalyst was characterized and observed by HITACHI H7650 transmission electron microscope (TEM) with the working voltage of 80 kV. High resolution transmission electron microscope (HRTEM) was performed by FEI Tecnai G2 F20 S-Twin with the 200 kV operating voltage and collected the elemental mappings with the assistance of X-ray energy dispersive spectroscopy detector. The crystalline structure and phase purity were identified using a D8 ADVANCE X X-ray powder diffractometer with CuKa radiation (λ = 1.5406 Å). The central metal loading of the Ni SA@N-$Ti_3C_2T_x$ were measured by Agilent ICP-OES 730. Atomic force microscopy (AFM) was used to characterize the thickness of nanosheets, and Bruker Dension Icon from Germany was used for testing. The atomic-resolution HAADF-STEM characterization was conducted using a probe aberration-corrected microscope, JEOL JEM-ARM200F equipped with cold emitter, an accelerating voltage of 200kV. X-ray photoelectron spectroscopy (XPS) was obtained by PerkinElmer Physics PHI 5300 energy spectrometer using mono-chromatic Al Kα radiation (1486.7 eV).

Ex-situ XAFS measurements.

The X-ray absorption fine structure spectra data (XAFS, Ni K-edge) were measured at BL1W1B station in Beijing Synchrotron Radiation Facility (BSRF, operated at 2.5 GeV with a maximum current of 250 mA). The XAFS data of all the samples were measured at room temperature in fluorescence excitation mode using a Lytle detector. All samples were prepared as plates of 13 mm diameter with 1mm thickness with the addition of graphite powder as a binder.

XAFS Analysis and Results.

The acquired EXAFS data were processed according to the standard procedures by using the ATHENA module of the IFEFFIT software packages. The detailed fitting process is stated below:

The obtained EXAFS spectra underwent the subtraction of post-edge background from the overall absorption and then normalization with respect to the edge-jump step. Subsequently, the χ(k) data were Fourier transformed to real (R) space by using a

hanning windows (dk=1.0 Å^{-1}) to separate the EXAFS contributions from different coordination shells. To obtain the quantitative structural parameters around central atoms, least-squares curve parameter fitting was conducted by using the ARTEMIS module of the IFEFFIT software packages.

The following EXAFS equation was used:

$$\chi(k)=\sum_j \frac{N_j S_o^2 F_j(k)}{k R_j^2}\exp[-2k^2\sigma_j^2]\exp[\frac{-2R_j}{\lambda(k)}]\sin[2kR_j+\phi_j(k)]$$

In the equation, S_0^2 represent the amplitude reduction factor, $F_j(k)$ is the effective curved-wave backscattering amplitude, N_j is the number of neighbors in the j^{th} atomic shell, R_j represent the distance between the X-ray absorbing central atom and the atoms in the j^{th} atomic shell (backscatterer), λ represent the mean free path in Å, σ_j is the Debye-Waller parameter of the j^{th} atomic shell (variation of distances around the average R_j) and $\phi_j(k)$ is the phase shift (including the phase shift for each shell and the total central atom phase shift). The functions $F_j(k)$, λ and $\phi_j(k)$ were calculated with the ab initio code FEFF8.2

The coordination numbers of model samples (Ni foil) were fixed as the nominal values. The obtained S_0^2 was fixed in the subsequent fitting of Ni SA@N-$Ti_3C_2T_x$ sample. While the internal atomic distances R, Debye-Waller factor σ^2, and the edge-energy shift ΔE_0 were allowed to run freely.

Electrochemical Measurements.

The electrochemical measurements were carried out on a CHI 760e electrochemical workstation in a three-electrode configuration cell using as-prepared electrode as the working electrode, graphite rod as the counter electrode, and Ag/AgCl (saturated KCl) as the reference electrode in 0.5 M H_2SO_4 aqueous electrolyte. To prepare a homogeneous ink, 4 mg of the sample and 10 μL of a 5 wt% Nafion solution were dispersed in 1 mL of a water-isopropanol solution with a 1:1 volume ratio, followed by 30 min sonication. Then 20 μL of the dispersion (containing 80 μg of catalyst) wasloaded onto a glassy carbon electrode (5 mm in diameter, catalyst loading 0.408 mg cm^{-2}). The LSV curves were conducted at scan rate of 20 mV/s.

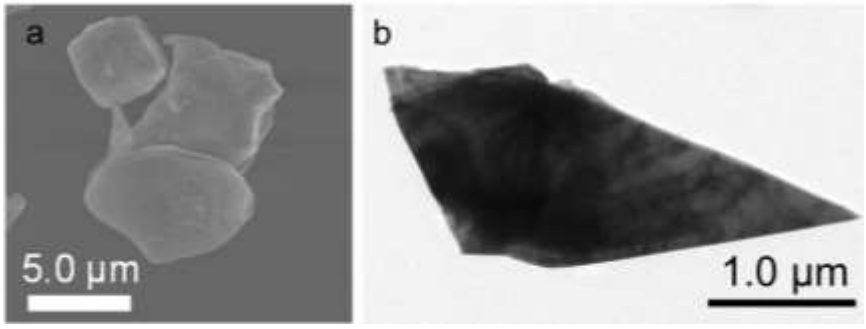

Figure S1. (a) TEM and (b) SEM image of Ti_3AlC_2.

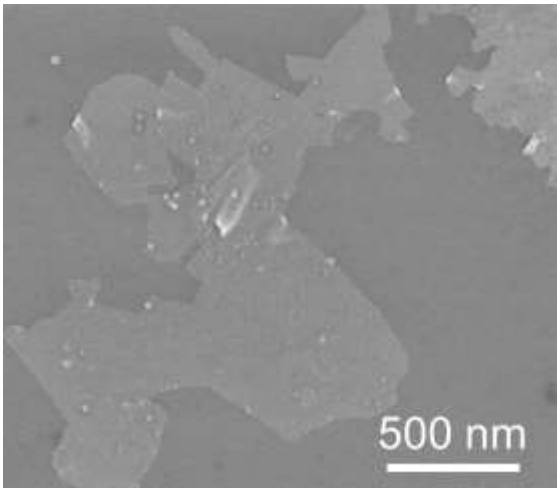

Figure S2. SEM image of $Ti_3C_2T_x$.

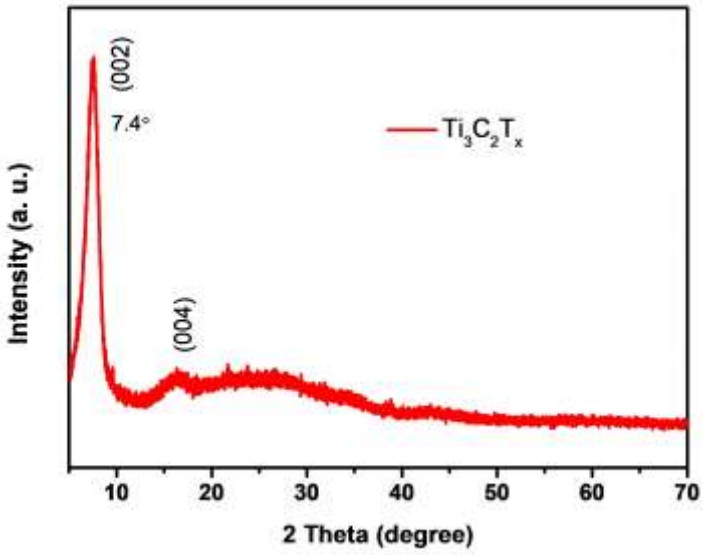

Figure S3. XRD pattern of $Ti_3C_2T_x$.

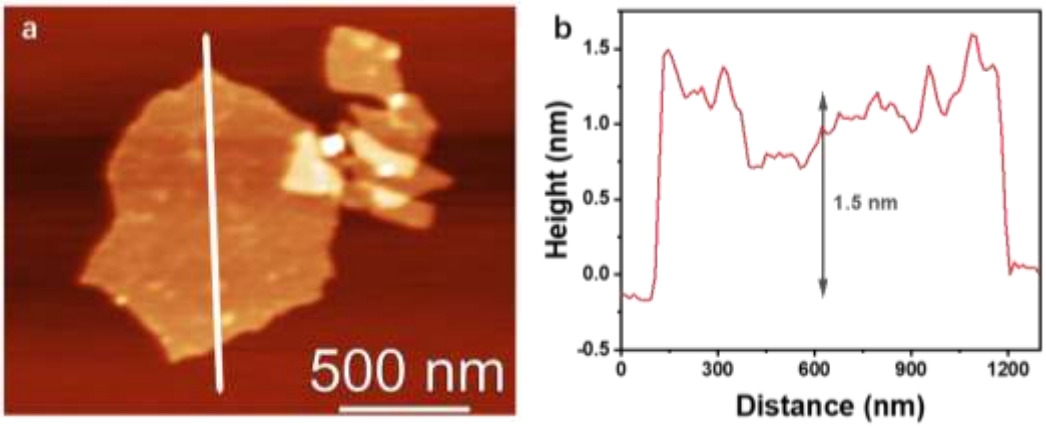

Figure S4. AFM image and its height curve of $Ti_3C_2T_x$.

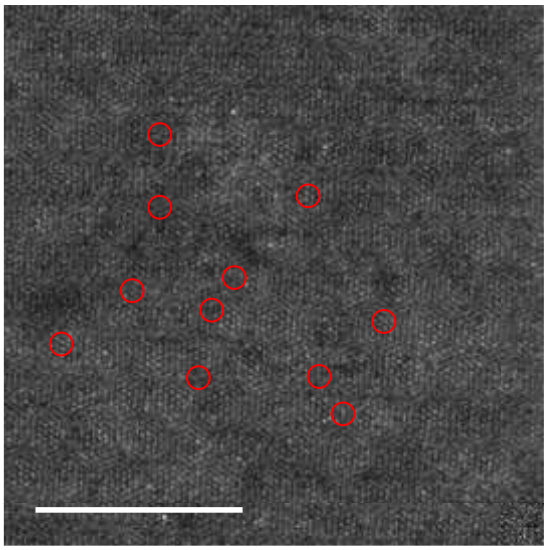

Figure S5. AC-HAADF-STEM image of $Ti_3C_2T_x$. The AC-HAADF-STEM image revealed the emerging of a large amount of Ti vacancies, which may act as ideal anchoring sites to immobile isolated metal atoms.

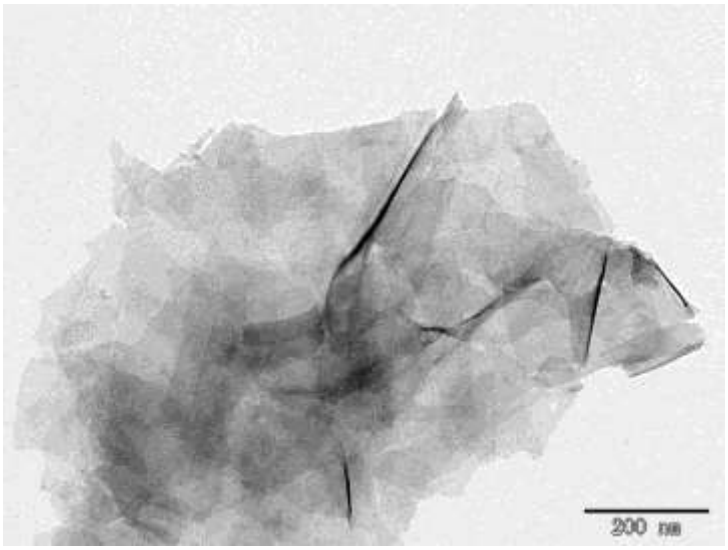

Figure S6. TEM pattern of Ni SA@N-$Ti_3C_2T_x$.

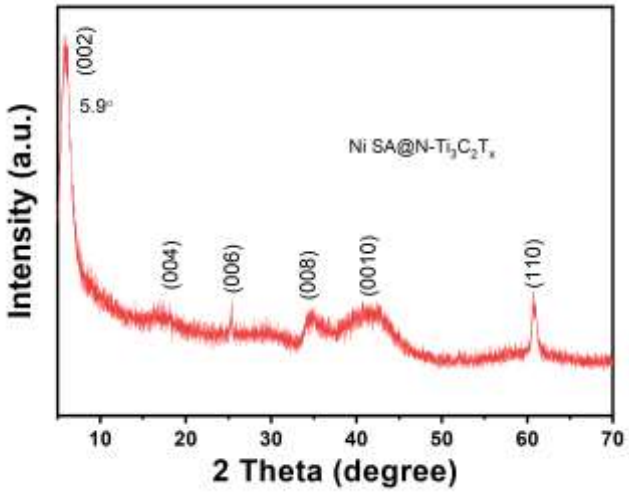

Figure 7. XRD pattern of Ni SA@N-$Ti_3C_2T_x$.

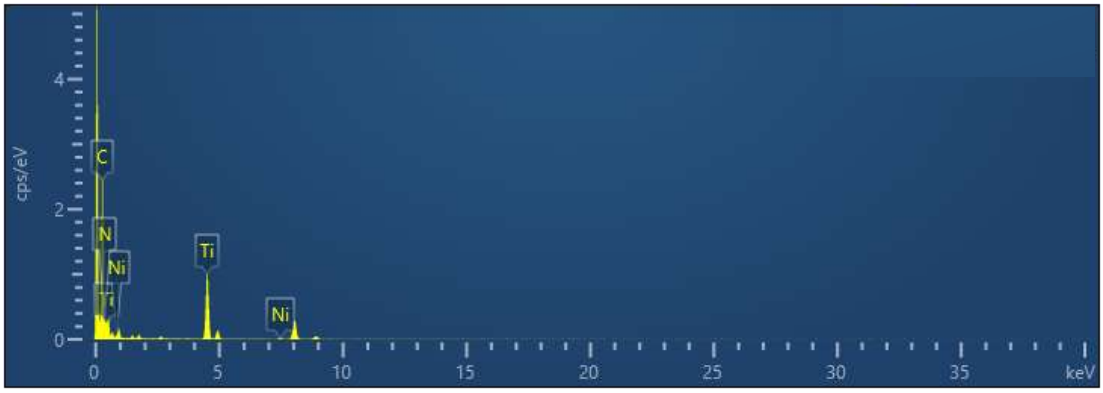

Figure S8. STEM EDX spectrum of Ni SA@N-$Ti_3C_2T_x$.

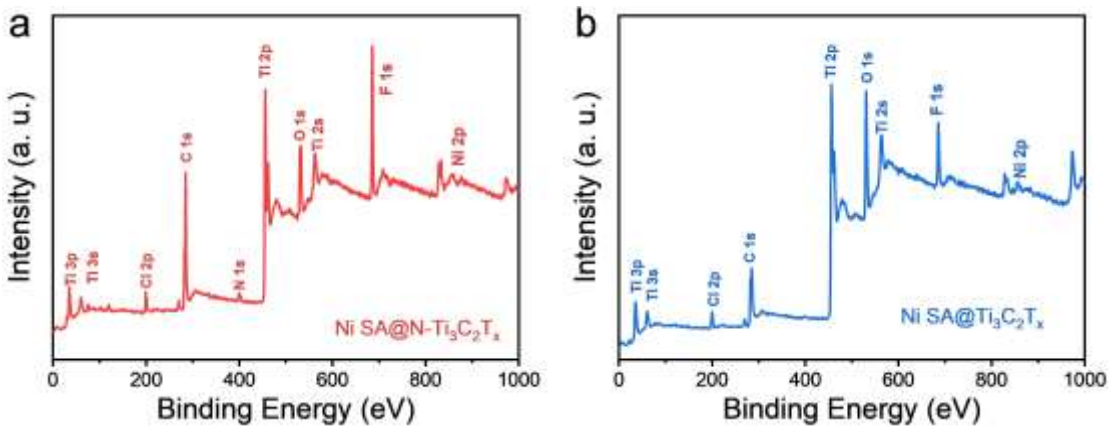

Figure S9. (a) XPS overall spectrum Ni SA@N-$Ti_3C_2T_x$. **(b)** XPS overall spectrum Ni SA@$Ti_3C_2T_x$. The survey spectrum of showed the existence of Ni, N, Ti, and C elements in Ni SA@N-$Ti_3C_2T_x$ (Fig. S9a). Moreover, Ni SA@$Ti_3C_2T_x$ showed the absence of N element in the Fig. S9b.

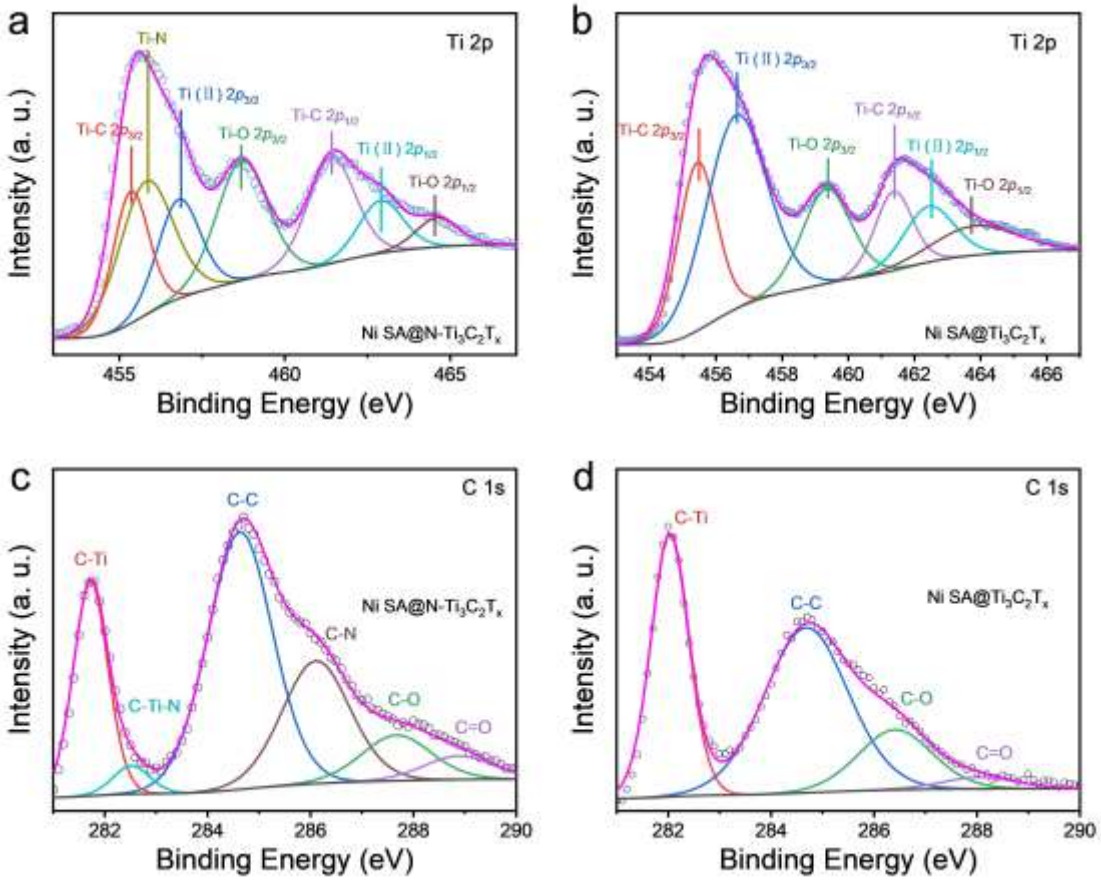

Figure S10. (a) High-resolution Ti 2*p* spectra of Ni SA@N-$Ti_3C_2T_x$. **(b)** High-resolution Ti 2*p* spectra of Ni SA@$Ti_3C_2T_x$. (**c**) High-resolution C 1*s* spectra of Ni SA@N-$Ti_3C_2T_x$. (**d**) High-resolution C 1*s* spectra of Ni SA@$Ti_3C_2T_x$. The high-resolution Ti 2*p* XPS spectra of Ni SA@N-$Ti_3C_2T_x$ displayed typical peaks at 455.3, 455.9, 456.8, 458.7, 461.4, 463.0 and 464.7 eV, which could be attributed to Ti-C $2p_{3/2}$,Ti-N, Ti(ll) $2p_{3/2}$, Ti-O $2p_{3/2}$, Ti-C $2p_{1/2}$, Ti(ll) $2p_{1/2}$, and Ti-O $2p_{1/2}$ bonds, respectively, and the Ti-N bonds was formed compared to that of Ni SA@$Ti_3C_2T_x$ (Fig. S10a and Fig. S10b). Meanwhile, the high-resolution C 1s spectra (Fig. S10c) of Ni SA@N-$Ti_3C_2T_x$ could be deconvoluted into C-Ti (281.7 eV), C-Ti-N (282.5 eV), C-C (284.6 eV), C-N (286.1 eV), C-O (287.7 eV) and C=O (288.9 eV). Furthermore, the C 1s spectra (Fig. S10d) of Ni SA@$Ti_3C_2T_x$ showed the absence of C-Ti-N and C-N, conforming the successful doping of N species and the electronic transfer between N and $Ti_3C_2T_x$.

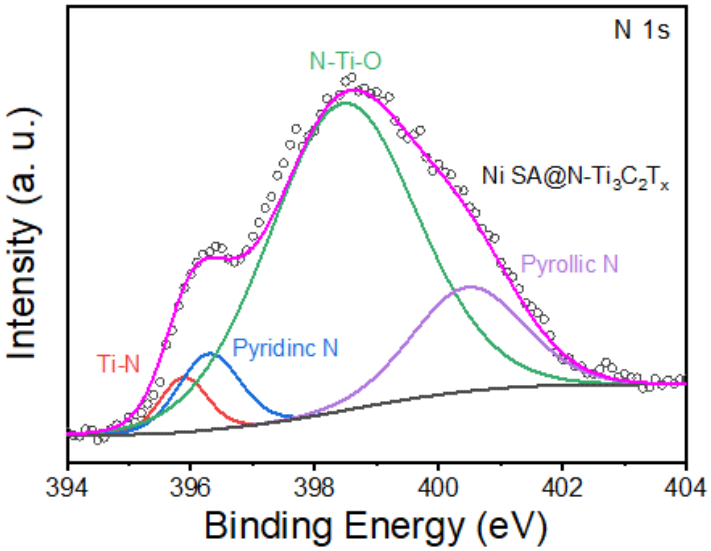

Figure S11. High-resolution N 1*s* spectra of Ni SA@N-$Ti_3C_2T_x$. Impressively, the N 1s spectra of Ni SA@N-$Ti_3C_2T_x$ showed the Ti-N and N-Ti-O bonds, providing the direct evidence for the interaction of N and $Ti_3C_2T_x$.

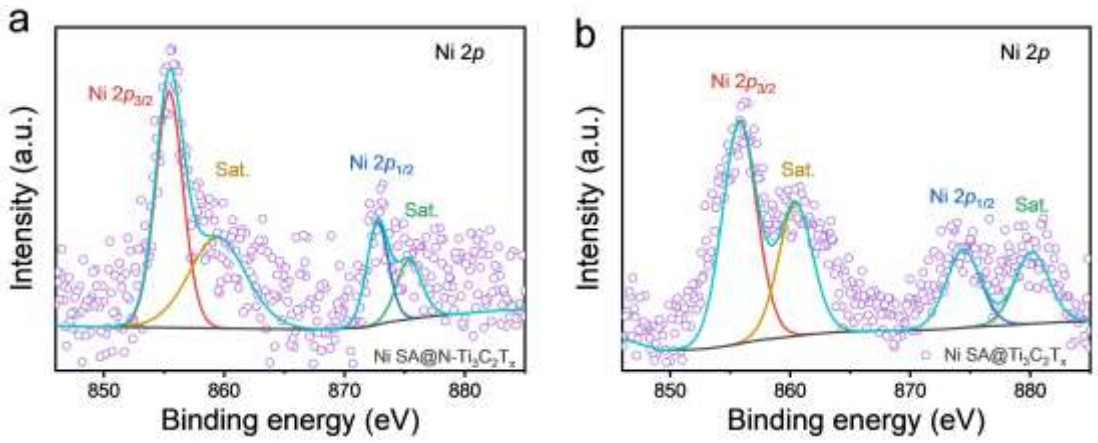

Figure S12. (a) High-resolution Ni 1*p* spectra of Ni SA@N-$Ti_3C_2T_x$. **(b)** High-resolution Ni 1*p* spectra of Ni SA@$Ti_3C_2T_x$. The Ni 2p spectrum of Ni SA@N-$Ti_3C_2T_x$ showed two obvious Ni(II) double peaks at 855.5 eV and 872.6 eV (Fig. S12), indicating the positively charged Ni species in Ni SA@N-$Ti_3C_2T_x$.

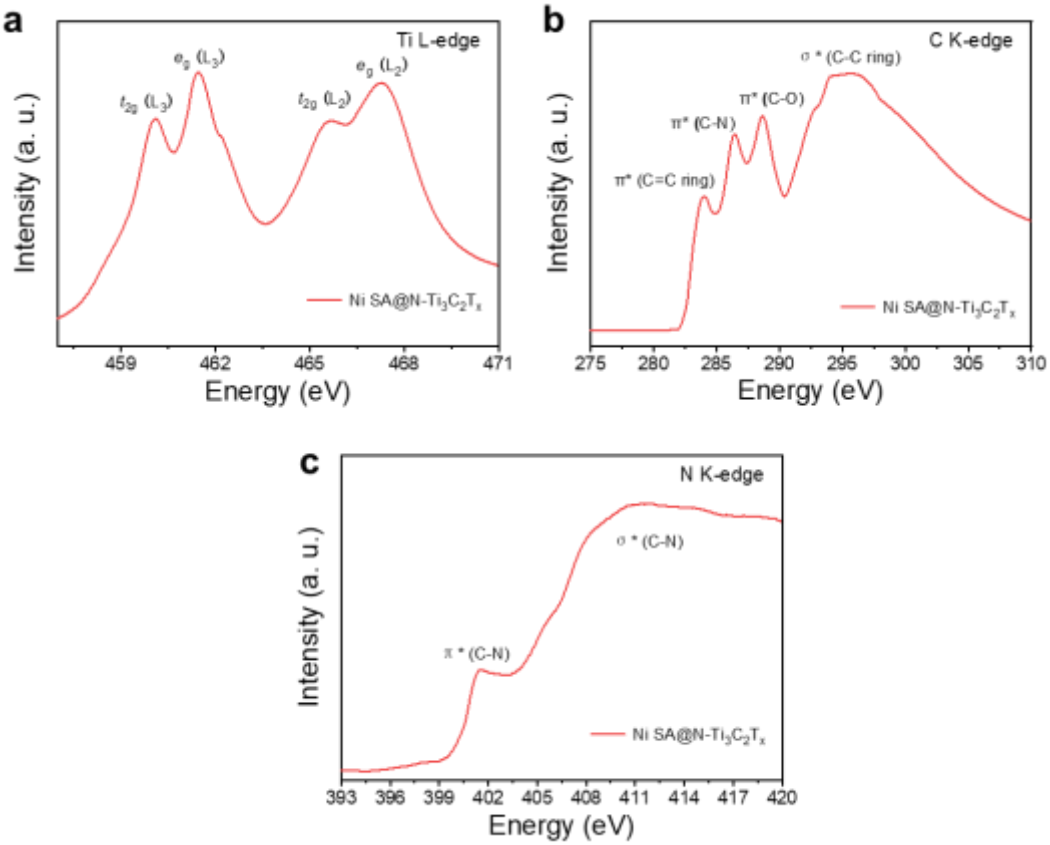

Figure S13. (a) Ti L-edge XANES spectra of Ni SA@N-$Ti_3C_2T_x$. **(b)** C K-edge XANES spectra of Ni SA@N-$Ti_3C_2T_x$. **(c)** N K-edge XANES spectra of Ni SA@N-$Ti_3C_2T_x$.

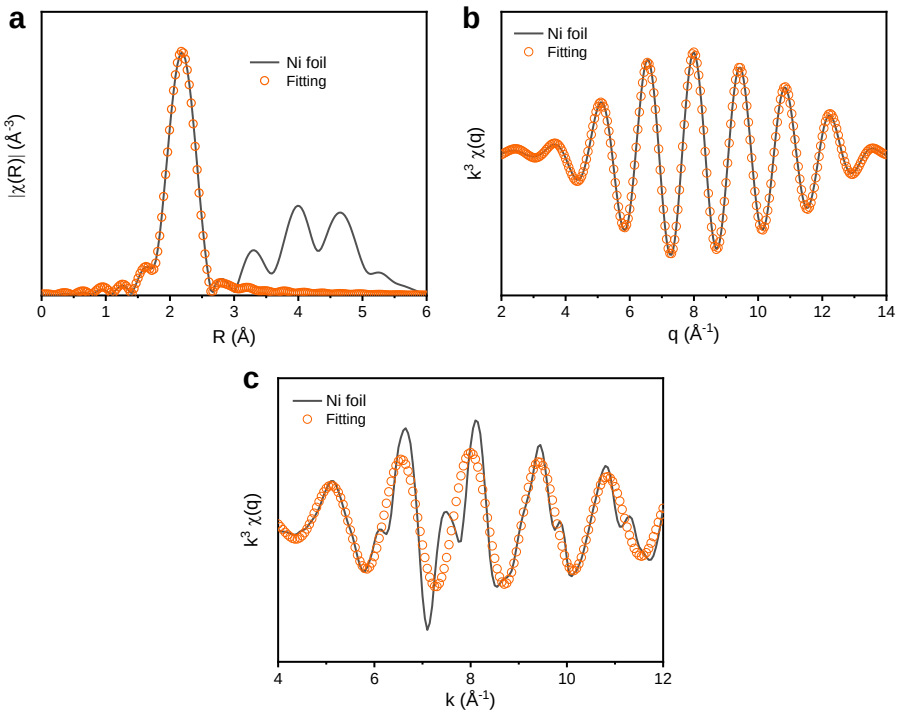

Figure S14. The EXAFS fitting results of Ni foil at (**a**) R, (**b**) q and (**c**) k space.

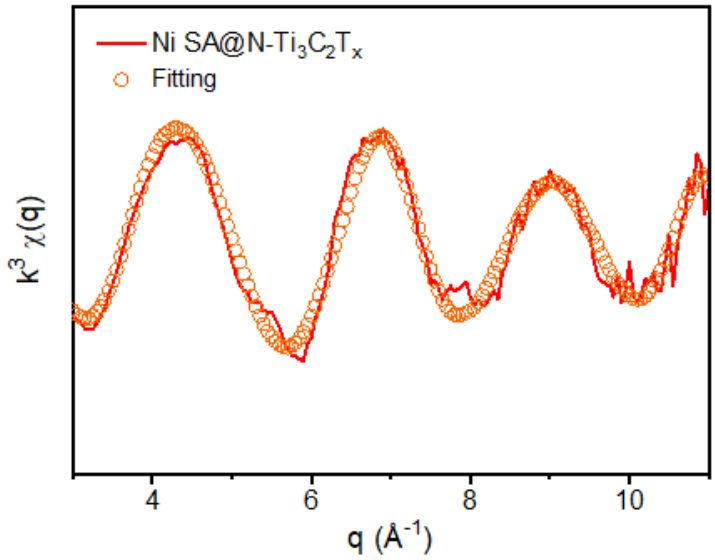

Figure S15. The EXAFS fitting results of Ni SA@N-$Ti_3C_2T_x$ at q space.

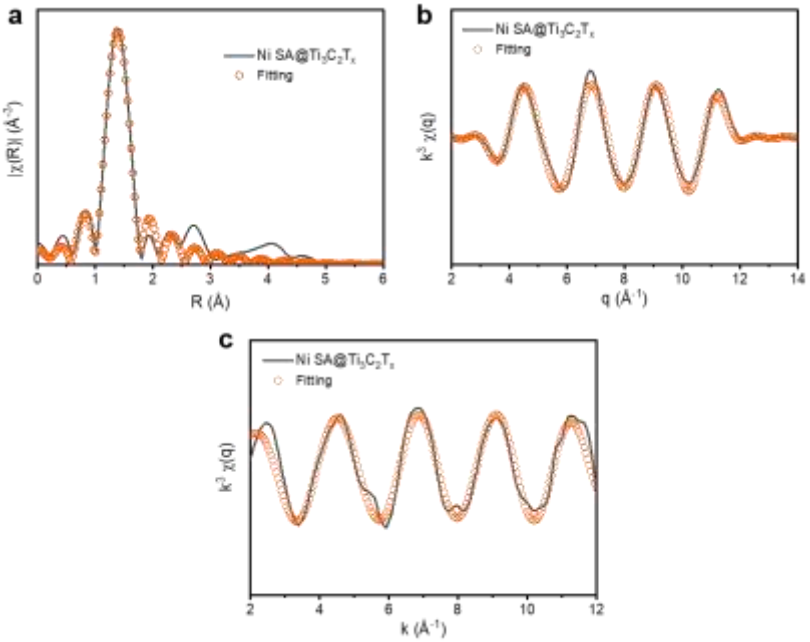

Figure S16. The EXAFS fitting results of Ni SA@$Ti_3C_2T_x$ at (**a**) R, (**b**) q and (**c**) k space.

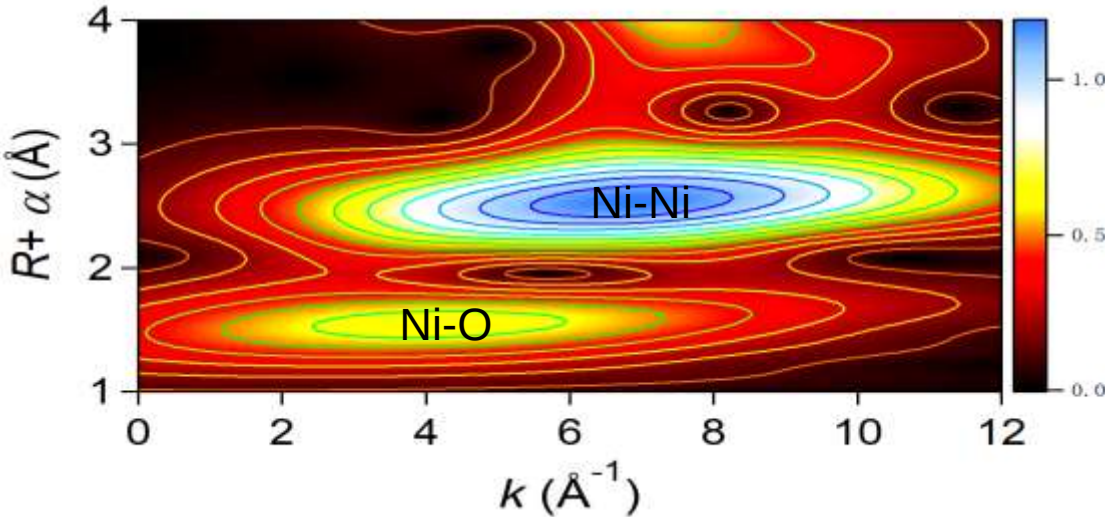

Figure S17. WT plot of NiO.

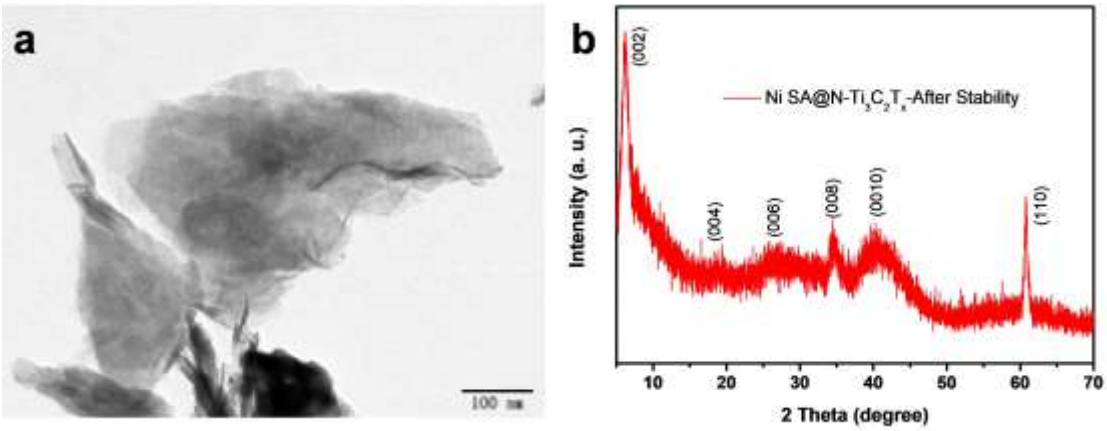

Figure S18. (a) TEM image of the of Ni SA@N-$Ti_3C_2T_x$ after stability testing. **(b)** XRD pattern of the of Ni SA@N-$Ti_3C_2T_x$ after stability testing.

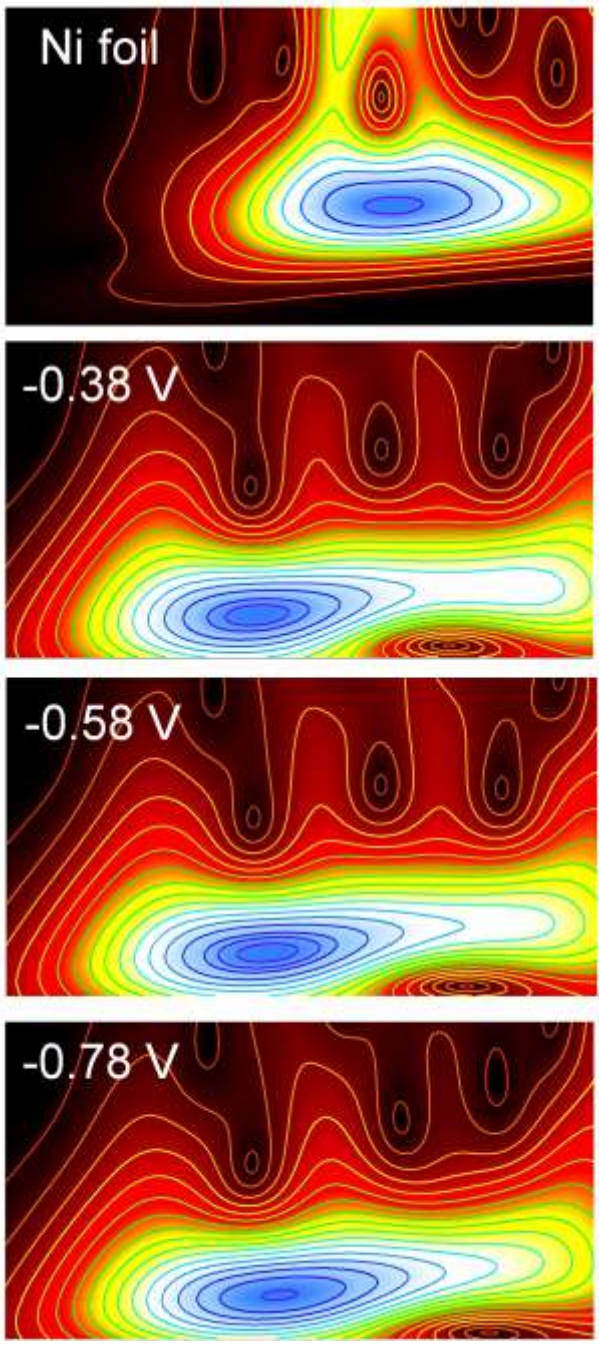

Figure S19. WT plot of Ni SA@N-$Ti_3C_2T_x$ at OCP and various potentials during HER.

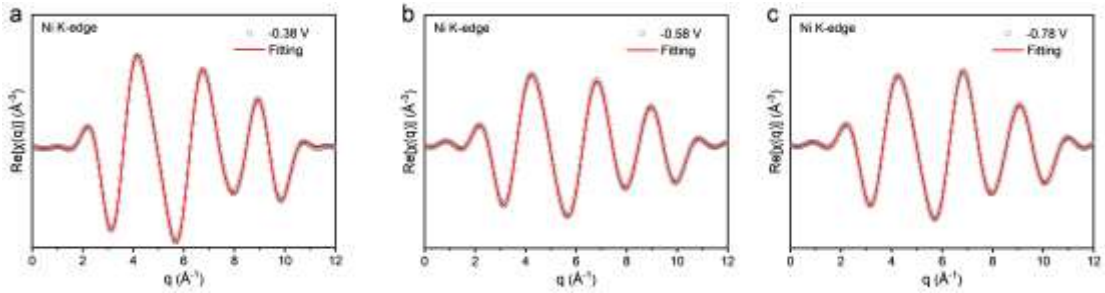

Figure S20. First-shell fitting of EXAFS spectra under -0.38, -0.58, and −0.78 V *vs.* RHE at q space.

Table S1. Structural parameters extracted from Ni K-edge EXAFS fitting. (S_0^2=0.84).

Sample	Path	CN	R(Å)	$\sigma^2(10^{-3}Å^2)$	ΔE_0(eV)	R factor
Ni SA@N-$Ti_3C_2T_x$	Ni-C	1.1	1.96	7.6	6.9	0.005
	Ni-N	1.0	1.98	9.5		
Ni SA@ $Ti_3C_2T_x$	Ni-C	2.1	1.97	7.6	8.5	0.008
Ni foil	Ni-Ni	12	2.49	6.2	7.2	0.002

S_0^2 is the amplitude reduction factor; CN is the coordination number; R is interatomic distance (the bond length between Ni central atoms and surrounding coordination atoms); σ^2 is Debye-Waller factor (a measure of thermal and static disorder in absorber-scatterer distances); ΔE_0 is edge-energy shift (the difference between the zero kinetic energy value of the sample and that of the theoretical model). R factor is used to value the goodness of the fitting.

* This value was fixed during EXAFS fitting, based on the known structure.

Error bounds that characterize the structural parameters obtained by EXAFS spectroscopy were estimated as N ± 20%; R ± 1%; σ^2 ± 20%; ΔE_0 ± 20%.